sustainability

MDPI

Article

Evaluation of Construction and Demolition Waste and Other Alternative Fills for Strip-Reinforced Soil Walls

Luis Alonso González Corrales [1], Rodrigo Cesar Pierozan [2], Gregório Luís Silva Araújo [3,*] and Ennio Marques Palmeira [3]

[1] Department of Geology, Central American School of Geology, University of Costa Rica, Ciudad Universitaria Rodrigo Facio, San José 214-2060, Costa Rica; luis.gonzalez_c@ucr.ac.cr
[2] Department of Civil Engineering, Federal Institute of Education, Science, and Technology of Rondonia, 4985 Calama Av., Porto Velho 76820-441, Brazil; rodrigo.pierozan@ifro.edu.br
[3] Department of Civil & Environmental Engineering, University of Brasilia, Darcy Ribeiro Campus, Brasilia 70910-900, Brazil; palmeira@unb.br
* Correspondence: gregorio@unb.br

Abstract: This article assesses the pullout performance of ribbed metallic strips embedded in fill soils that do not conform to conventional design criteria for mechanically stabilized earth (MSE) walls. These alternative fill soils include gravelly and sandy recycled aggregates from construction and demolition waste, artificial and natural sands, and fine-grained lateritic soil. The research included soil characterization tests and large-scale pullout tests, conducted as part of this study. The results showed that the reinforcement pullout behavior was similar for recycled, artificial, and natural sands, indicating that soil particle size played a crucial role in mobilizing the interface pullout resistance. However, in the case of recycled sand, stress concentration at the reinforcement level led to particle crushing during pullout conditions, causing this material to exhibit less efficient performance compared to other sands. The fine-grained lateritic soil demonstrated inferior behavior compared to sandy soils, despite the interparticle bonding provided by the sesquioxide coating characteristic of intensely weathered tropical soils. Finally, an analytical prediction tool based on experimental results was developed, providing an alternative method to make conjectures about the performance of different soils during the pre-design stages, particularly based on particle size attributes.

Keywords: recycled construction and demolition waste; alternative fill materials; lateritic soil; pullout; mechanically stabilized earth walls

Citation: Corrales, L.A.G.; Pierozan, R.C.; Araújo, G.L.S.; Palmeira, E.M. Evaluation of Construction and Demolition Waste and Other Alternative Fills for Strip-Reinforced Soil Walls. *Sustainability* **2023**, *15*, 9705. https://doi.org/10.3390/su15129705

Academic Editor: Fernanda Bessa Ferreira

Received: 17 May 2023
Revised: 10 June 2023
Accepted: 15 June 2023
Published: 17 June 2023

1. Introduction

Mechanically stabilized earth (MSE) walls utilize the tensile capabilities of inclusions to create reinforced soil masses, and their geomechanical performance is influenced by fill quality and reinforcement characteristics, with coarse-grained aggregates being preferred over fine-grained soils [1–5]. This has limited the use of some alternative fill materials in MSE walls, such as fine-grained tropical soils and industrial byproducts [6], which often do not achieve the conventional design criteria [7–12].

Utilizing industry byproducts in engineering works can enhance the energy efficiency and provide benefits from social, technical, economic, and environmental perspectives. For example, scrap tire strips are a feasible alternative for soil reinforcement [13], and recycled aggregates from construction and demolition waste (CDW) have been successfully used in cementitious materials, in road pavement layers, and as backfills in retaining walls [14–26]. However, a more insightful understanding of their performance in terms of soil-reinforcement resistance mechanisms is needed for further applications as fills in MSE walls due to the existing deficiencies in design procedures and technical literature relative to this usage [27,28].

The use of fine-grained tropical soils as fills in MSE walls could also contribute to cost-effective projects, given their large availability in tropical and subtropical climate zones [29–31]. Previous studies have shown that the micro-structural bonding caused by an accumulation of sesquioxides (iron and aluminum oxides) between soil particles may induce relevant changes in geomechanical responses relative to fine-grained soils found in temperate regions [30,32,33], enhancing the geomechanical responses of lateritic soil subgrades in natural conditions or after soil stabilization [34–38]. However, concerns related to fine-grained soil compressibility and reduced interface resistance have inhibited further applications as fills in MSE walls [39–41], which could be partially addressed with studies that consider the particularities of tropical soils.

This paper examines the pullout results of metallic strips embedded in various fill materials for use in MSE walls, including coarse-grained recycled aggregates from CDW (both gravelly and sandy), artificial and natural sands, and an intensely weathered fine-grained silty material from a natural deposit. The primary contribution of this work to the field of geotechnical engineering lies in the potential utilization of materials that do not meet the design requirements for MSE walls reinforced with strips but can still exhibit good performance and cost-effectiveness, particularly in the context of limited natural resources that has become increasingly critical. Information about the soils tested is presented, along with details on the pullout testing procedures. Results are analyzed from a design standpoint, and the findings provide an analytical tool for considering the unique characteristics of the tested soils.

2. Soil Characterization

The research utilized CDW obtained from an authorized treatment plant located in Brasilia (Federal District, Brazil). The plant undertakes the recycling of debris obtained from the demolition of residential buildings, which involves the removal of impurities such as plastics, metals, wooden materials, glass, and soil. The CDW was graded and combined after purification, and gravimetric composition analysis was performed. The assessment established that concrete (30.7% in mass), unbound aggregates (22.3% in mass), natural stone (15.2% in mass), mortar (12.5% in mass), masonry (10.2% in mass), ceramics (8.6% in mass), and other (0.5% in mass) were the most prominent constituents of the recycled CDW. In this investigation, two samples were collected from this material, namely, recycled gravel (RG) and recycled sand (RS), with particle diameters (D) in the range of 2 mm $< D \leq$ 10 mm and 0 $< D \leq$ 2 mm, respectively.

This study also included artificial sand (AS) sourced from a quartzite quarry facility located in Brasilia (Federal District, Brazil), natural sand (NS) extracted from a fluvial deposit at Rio das Almas (State of Goias, Brazil), and lateritic soil (LS) collected from the Experimental Field of the University of Brasilia Geotechnical Engineering Graduate Program (Federal District, Brazil), which is a heavily weathered tropical soil [5]. To eliminate the possibility of influencing test results, soil particles with D larger than 2 mm were removed from AS, NS, and LS.

2.1. Chemical and Mineralogical Properties

The chemical and mineralogical composition of fill soils were evaluated using the X-ray fluorescence (XRF) and X-ray diffraction (XRD) techniques, respectively. Figure 1 summarizes the test results, with Figure 1a showing the chemical analyses and Figure 1b presenting the mineral composition. As the samples of RG and RS were extracted from the same recycled CDW sample, the chemical and mineralogical analyses presented in Figure 1 represent the results of a single sample for these two materials.

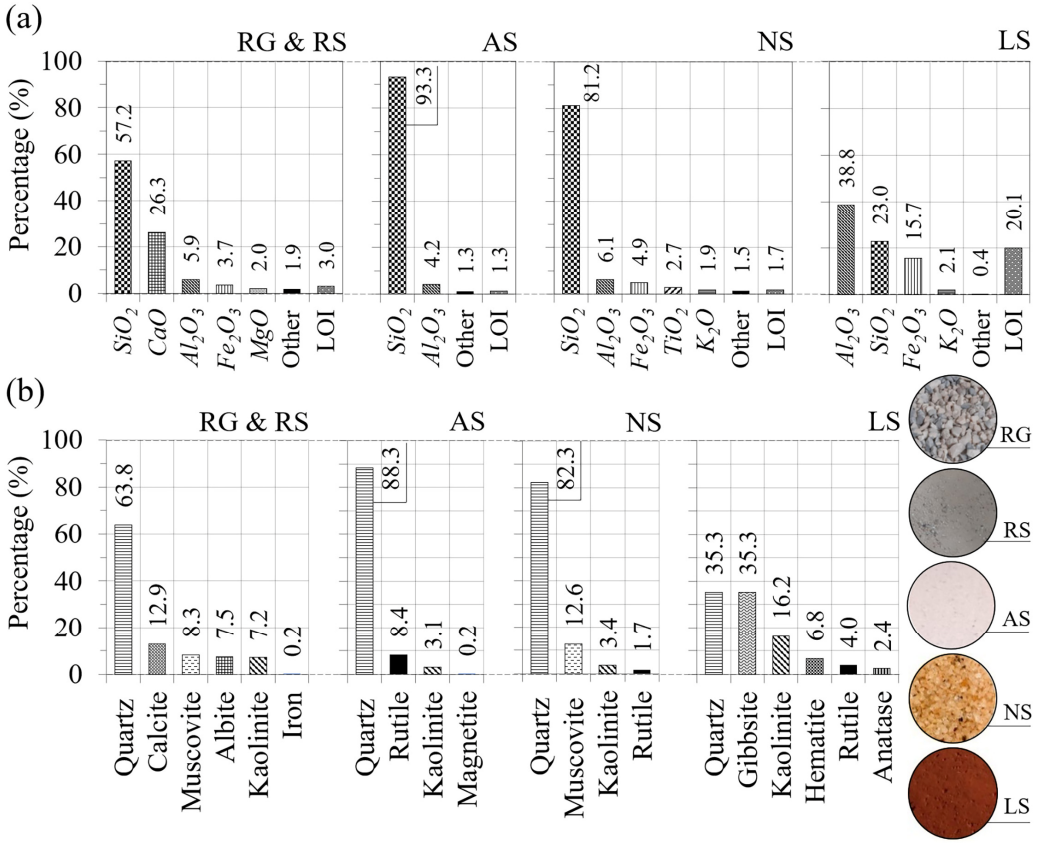

Figure 1. XRF and XRD test results for: (**a**) chemical components, and (**b**) minerals. Note: Chemical components shown in (**a**) include aluminum oxide (Al_2O_3), calcium oxide (CaO), ferric oxide (Fe_2O_3), magnesium oxide (MgO), potassium oxide (K_2O), silicon dioxide (SiO_2), and titanium dioxide (TiO_2).

Chemical analyses [Figure 1a] reveal that RG and RS are primarily composed of silica (SiO_2, 57.2%) and calcium oxide (CaO, 26.3%), with secondary components such as alumina (Al_2O_3), iron oxide (Fe_2O_3), and magnesium oxide (MgO) accounting for 11.6% of the total mass. AS also contains 4.2% of Al_2O_3, while NS contains 15.6% of Al_2O_3, Fe_2O_3, titanium oxide (TiO_2), and potassium oxide (K_2O). LS contains significant amounts of Al_2O_3 (38.8%), SiO_2 (23.0%), and Fe_2O_3 (15.7%), with 2.5% of other components. To incorporate a variable related to the chemical composition of tropical soils in subsequent analyses, the silica–sesquioxides ratio parameter was calculated for all samples based on the following equation [42]:

$$SSR = S \times (A + F)^{-1} \quad (1)$$

where *SSR* stands for the silica–sesquioxides ratio, which can be calculated using the percentages of chemical components denoted by *S*, *A*, and *F*. The percentages are calculated as $\%SiO_2/60$, $\%Al_2O_3/102$, and $\%Fe_2O_3/160$, respectively.

It is worth noting that *SSR* represents the relative proportion between silica (SiO_2), a stable mineral with desirable properties for MSE wall fill materials, and oxides commonly associated with soil weathering (Al_2O_3 and Fe_2O_3). *SSR* values of 11.861, 35.737, 14.966, and 0.801 were determined for the RG and RS, AS, NS, and LS samples, respectively. Notably, the difference in *SSR* values between the granular materials (RG, RS, AS, and NS) and LS suggests that the latter underwent significant weathering, which could result in substantial differences in geomechanical responses compared to other tested samples.

The most relevant minerals present in RG and RS were quartz (SiO_2, 63.8%), calcite ($CaCO_3$, 12.9%), and muscovite [$(K,Na)(Al,Mg,Fe)_2(Si_{3.1}Al_{0.9})O_{10}(OH)_2$, 8.3%]. On the other hand, AS was mostly composed of quartz (88.3%), with rutile (TiO_2, 8.4%), kaolinite [$Na_{0.3}Al_4Si_6O_{15}(OH)_{6.4}H_2O$, 3.1%], and magnetite ($Fe_3O_4$, 0.2%) as secondary minerals.

NS was also mostly composed of quartz (82.3%), with muscovite (12.6%), kaolinite (3.4%), and rutile (1.7%) present. LS was primarily composed of quartz (35.3%) and gibbsite [$Al_2(OH)_3$, 35.3%], with secondary components including kaolinite (16.2%), rutile (4.0%), and anatase (2.4%).

2.2. Morphometric Analyses

Images collected using optical microscopy techniques were used as a reference for conducting qualitative morphometric analyses. Regarding the CDW aggregates (RG and RS), the analyses showed highly angular and rough surfaces on the CDW aggregates, with the presence of horizontal planes observed in some aggregates, originated from finished surfaces. When considering the different constituents of the CDW aggregates, it was not possible to detect significant differences in particle size in terms of the different constituents collected in each fraction (i.e., concrete, unbound aggregates, natural stone, mortar, masonry, and ceramics). AS sand exhibited an intermediate degree of sphericity and subangular surfaces, possibly resulting from quartzite quarrying. NS analyses showed lower surface roughness than AS, although subangular surfaces and intermediate sphericity were still present.

To better understand the micromorphological characteristics of the fill soils, scanning electron microscopy (SEM) analyses were conducted on all tested soils, and 3D X-ray microscopy and petrographic analysis were performed on the RG and AS, respectively. The selected results are presented in Figure 2. In the case of RG, Figure 2a shows a three-dimensional morphological representation of an RG aggregate. The presence of sub-horizontal planes from the original structure and small cavities from aggregates that detached during the recycling process are evident. Additionally, SEM analyses of the RG particles [Figure 2b] revealed the presence of cracks, which may be linked to their heterogeneous composition and the influence of the recycling process. These cracks could impact the performance of these aggregates under service conditions. Indeed, prior research [25,43,44] has associated the loss of CDW aggregate performance with the possibility of particle breakage, particularly in larger aggregates such as the RG employed in this study. An overall rough surface was also observed for RG.

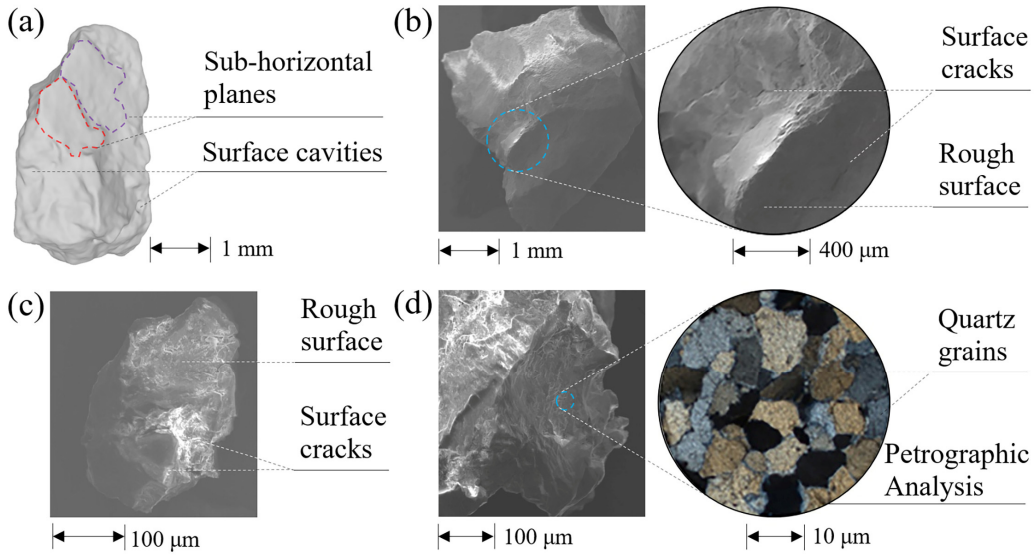

Figure 2. Morphometric characteristics of soils: (**a**) a 3D representation of RG indicating its primary surface features, (**b**) SEM analysis of RG revealing surface cracks and roughness, (**c**) the same analysis for RS, and (**d**) SEM and petrographic analysis of AS, highlighting the presence of well-defined quartz grains resulting from metamorphism.

Based on Figure 2c, it was also possible to detect the presence of surface cracks in the case of RS, similar to those observed in RG, along with a rough surface. Conversely, for AS, a rough surface without the presence of cracks was observed, as shown in Figure 2d. This could result in the better performance of these materials as fill compared to CDW aggregates. Additionally, petrographic analysis was performed using AS, indicating a significant presence of quartz grains consistent with the results of mineralogical characterization. Furthermore, the presence of well-structured grains evidences the metamorphic nature of quartzite, which could attribute a greater strength to this material compared to other aggregates.

Results for NS and LS were not presented in this study as they are available in [45]. It is worth noting that NS presented intact grains without surface cracks, while LS aggregates ranging from 50 µm to 150 µm had angular and rough surfaces attributed to the sesquioxide coating provided by iron and aluminum oxides. This is in line with the high *SSR* value assigned to LS, as described in the previous section.

2.3. Geomechanical Properties

The specific gravity of soil solids was determined following [46]. Accordingly, Ref. [47] was used as a reference to determine the dimensions of individual particles in soils RG, RS, AS, and NS. For soil LS, the dimensions of individual particles were determined using conventional testing procedures, which involve solution stirring and the use of a dispersing agent (DA), as per [48], while the dimensions of soil aggregations were determined via [49], without solution stirring and DA. Vibratory table tests [50] and funnel tests [51] were conducted for gravelly and sandy soil samples (RG, RS, AS, and NS), while Proctor compaction tests [52] were carried out for soil LS. Additional tests included the evaluation of Atterberg limits [53] for soil LS, and the resistance to degradation of coarse aggregates using the Los Angeles machine [54] for soil RG. Table 1 summarizes the test results and relevant additional information.

Based on the results in Table 1, the recycled aggregates had solid densities (G_s) of 2.66 and 2.68 for RG and RS, respectively, while the values for the AS, NS, and LS soils were 2.71, 2.64, and 2.67, respectively. It is worth noting that the relatively high G_s of AS is due to the presence of rutile and magnetite in its mineralogical composition [Figure 1b]. Only LS exhibited plasticity, with a plasticity index (*PI*) of 11%, and RG showed 34% abrasion losses during the Los Angeles machine test. The corresponding sizes for 10%, 30%, 50%, and 60% of the passing soil fraction were also determined. RG, RS, AS, and NS had C_c values of 1.40, 1.24, 0.89, and 0.97, respectively, while their corresponding C_u values were 1.83, 2.90, 2.06, and 2.38. However, LS had C_c and C_u values of around 5 and 25, respectively, when considering individual soil particle sizes, and 10.21 and 53.33, respectively, when considering soil agglomerations rather than individual particle dimensions.

Table 1 also presents the fines content (F_c) for RG, NS, RS, and AS, which represents the mass fraction of soil particles with a diameter smaller than 0.075 mm. RG and NS had F_c close to zero, while RS and AS had 4.2% and 1.1% of fines, respectively. LS had a high F_c of 64.8% based on individual soil particle sizes, but the F_c was reduced to 31.4% for soil agglomerations. RG was classified as poorly graded gravel (GP) while RS, AS, and NS were classified as poorly graded sands (SP) according to the Unified Soil Classification System [55]. Based on the particle size distribution of individual soil particles, LS was classified as a low plasticity silt (ML). However, considering the dimensions of agglomerations, LS could be classified as silty sand (SM). These findings suggest that the sesquioxide coating significantly impacts the structure of intensely weathered tropical soils, specifically LS, giving them an aggregated structure similar to that of sand under field conditions.

Table 1. Summary of geotechnical properties of tested soil samples and relevant additional information.

Soil Property	Fill Soils				
	RG	**RS**	**AS**	**NS**	**LS**
G_s (-)	2.66	2.68	2.71	2.64	2.67
w_L (-)	-	-	-	-	0.39
w_P (-)	-	-	-	-	0.28
PI (-)	-	-	-	-	0.11
LA (-)	0.34	-	-	-	-
D_{10} (mm)	3.0	0.10	0.17	0.29	<0.001 (0.003 *)
D_{30} (mm)	4.8	0.19	0.23	0.44	<0.001 (0.07 *)
D_{50} (mm)	5.0	0.25	0.30	0.60	0.02 (0.12 *)
D_{60} (mm)	5.5	0.29	0.35	0.69	0.06 (0.16 *)
C_c (-)	1.40	1.24	0.89	0.97	~5 (10.21 *)
C_u (-)	1.83	2.90	2.06	2.38	~25 (53.33 *)
F_c (-)	0.000	0.042	0.011	0.000	0.648 (0.314 *)
Unified Soil Classification System (USCS)	GP	SP	SP	SP	ML (SM *)
e_{max} (-)	1.06	0.98	1.01	0.83	-
e_{min} (-)	0.81	0.59	0.65	0.58	-
$\gamma_{d,max}$ (kN/m^3)	-	-	-	-	15.70
$w_{opt.}$ (-)	-	-	-	-	0.22
SSR (-)	11.861	11.861	35.737	14.966	0.801

(*) indicates results obtained from hydrometer tests conducted without a dispersing agent. Table 1 lists various symbols and their corresponding definitions for different properties of soil, including the specific gravity of solids (G_s), liquid limit (w_L), plastic limit (w_P), plasticity index (PI), Los Angeles abrasion index (LA), diameters corresponding to different levels of soil passing (D_{10}, D_{30}, D_{50}, and D_{60}), coefficients of curvature (C_c) and non-uniformity (C_u), fines content (F_c), maximum and minimum void ratios (e_{max} and e_{min}), maximum dry unit weight ($\gamma_{d,max}$), optimum water content (w_{opt}), and the silica–sesquioxides ratio (SSR).

Table 1 also shows that moisture played a crucial role in achieving maximum compaction for LS, with an optimal water content (w_{opt}) of 22% and a maximum dry unit weight ($\gamma_{d,max}$) of 22 kN/m^3. In contrast, the granular soils (RG, RS, AS, and NS) achieved their most compact state through vibration alone.

Figure 3 illustrates a comparison of the particle size distribution curves of the various materials with the recommended gradation limits according to the Federal Highway Administration (FHWA) [8], the National Concrete Masonry Association (NCMA) [12], and the British Standard Institution (BSI) [11], which are often considered as references for the design of MSE walls. RG lacks fine particles to fill the gaps between larger gravel particles, while the internal structure of the sands (RS, AS, and NS) could benefit from the presence of larger aggregates, which could significantly enhance the geomechanical behavior of these soils. Lastly, LS showed a fine particle size distribution when considering individual particles, which was partially altered when considering the dimensions of soil aggregates. Since none of the tested materials meet the conventional specifications for MSE wall backfill in terms of their texture, the materials herein investigated are evaluated as alternative fills when it comes to their pullout behavior.

The compaction requirements for MSE wall backfill materials suggested by FHWA [8] were followed for sample preparation, as summarized in Table 2. Granular samples (RG, RS, AS, and NS) were compacted to a relative density (I_d) of approximately 95%, while LS was compacted to a degree of compaction (D_c) of 95%. The moisture contents used for soil sample preparation (w_{target}) were equivalent to the hygroscopic moisture contents for granular soils (RG, RS, AS, and NS), while for LS, the value of w_{opt} (optimum water content) was used with a tolerance of ±2% relative to that value. Based on these parameters, the

corresponding testing conditions were established in terms of dry unit weights ($\gamma_{d,target}$) and bulk unit weights ($\gamma_{b,target}$), as well as the corresponding void ratios.

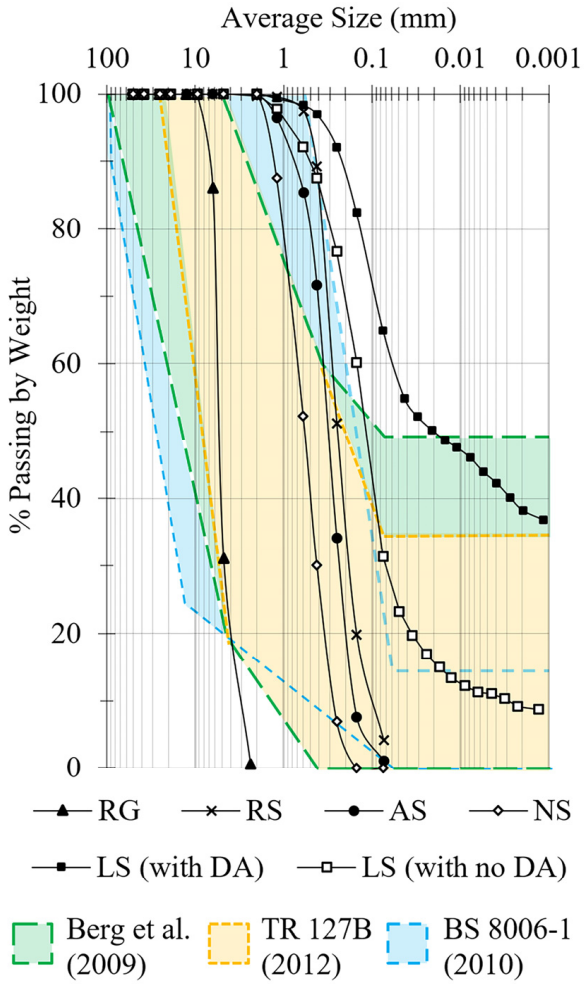

Figure 3. Particle size distribution curves and reference grading limits [8,11,12].

Table 2. Compaction criteria used for direct shear and pullout tests and the corresponding geomechanical properties of fill soils.

Soil Property	Fill Soils				
	RG	RS	AS	NS	LS
I_d (-)	0.952	0.961	0.963	0.950	-
D_c (-)	-	-	-	-	0.950
w_{target} (-)	0.01	0.03	0.03	0.03	0.22
$\gamma_{d,target}$ (kN/m^3)	15.30	16.28	15.98	16.30	14.91
$\gamma_{b,target}$ (kN/m^3)	15.45	16.77	16.46	16.79	18.19
e_{target} (-)	0.82	0.61	0.67	0.59	0.76
ϕ_s (degrees)	50	43	45	44	33
c_s (kPa)	0	4	0	0	30

Table 2 symbols are the following: relative density (I_d), degree of compaction (D_c), target water content of soil (w_{target}), target dry unit weight of soil ($\gamma_{d,target}$), target bulk unit weight of soil ($\gamma_{b,target}$), target void ratio of soil (e_{target}), soil friction angle (ϕ_s), and cohesion intercept of the soil shear resistance (c_s).

Table 2 also displays the geomechanical properties of compacted specimens (unsaturated) with dimensions of 100 mm × 100 mm × 20 mm, which underwent direct shear tests [56] to evaluate the shear resistance of RS, AS, NS, and LS. For RG, the same test was conducted, but larger samples were utilized in a larger equipment having internal dimensions of 300 mm in all three directions. Friction angles (ϕ_s) for RG, RS, AS, NS, and LS were equal to 50°, 43°, 45°, 44°, and 33°, respectively, based on the test results and Mohr–Coulomb strength criterion. The cohesive intercepts (c_s) for all materials were close to zero, except for RS and LS which had cs values of 4 kPa and 30 kPa, respectively.

3. Pullout Tests

Figure 4 displays photographs of the equipment used for pullout testing, including a side view of the equipment and the acrylic wall that allows a visualization of the compaction quality [Figure 4a], the sand rain procedure used for sand compacity control [Figure 4b], and the mechanical hammer used for soil compaction [Figure 4c]. Double layers of lubricant and polyethylene film were applied to the internal surfaces of the pullout box in order to minimize sidewall friction. Additional details regarding the compaction procedures are presented later in this section.

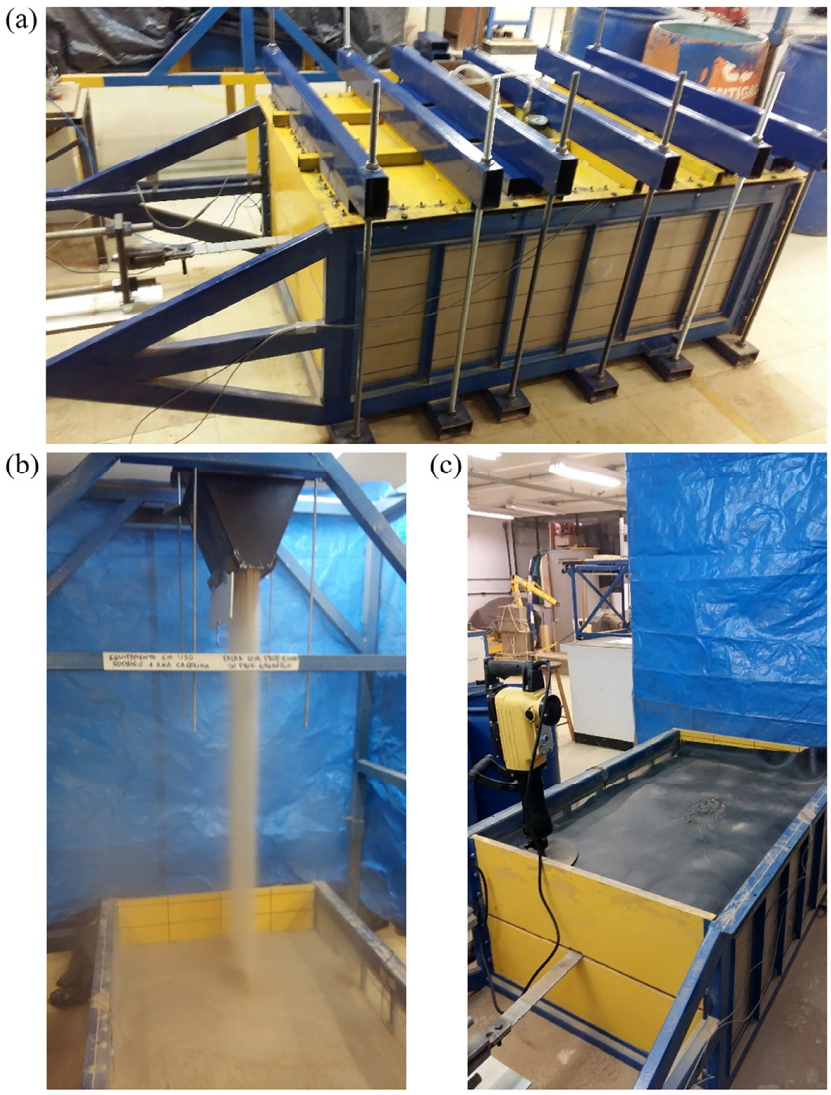

Figure 4. Photographs of the pullout equipment employed in this study: (**a**) side view of the pullout box, (**b**) sand rain procedure, and (**c**) soil compaction using a mechanical hammer.

To provide a better understanding of the dimensions of the pullout equipment and its related components, Figure 5 provides a detailed view of the pullout apparatus utilized in this study. Its internal dimensions measure 1450 mm (length), 890 mm (width), and 570 mm (height). Figure 5a illustrates the placement of the reinforcement element and instrumentation, comprising one (1) load cell and two (2) displacement transducers, positioned at the load application point, and connected to a data acquisition system. The system for applying horizontal loads consisted of a hydraulic cylinder.

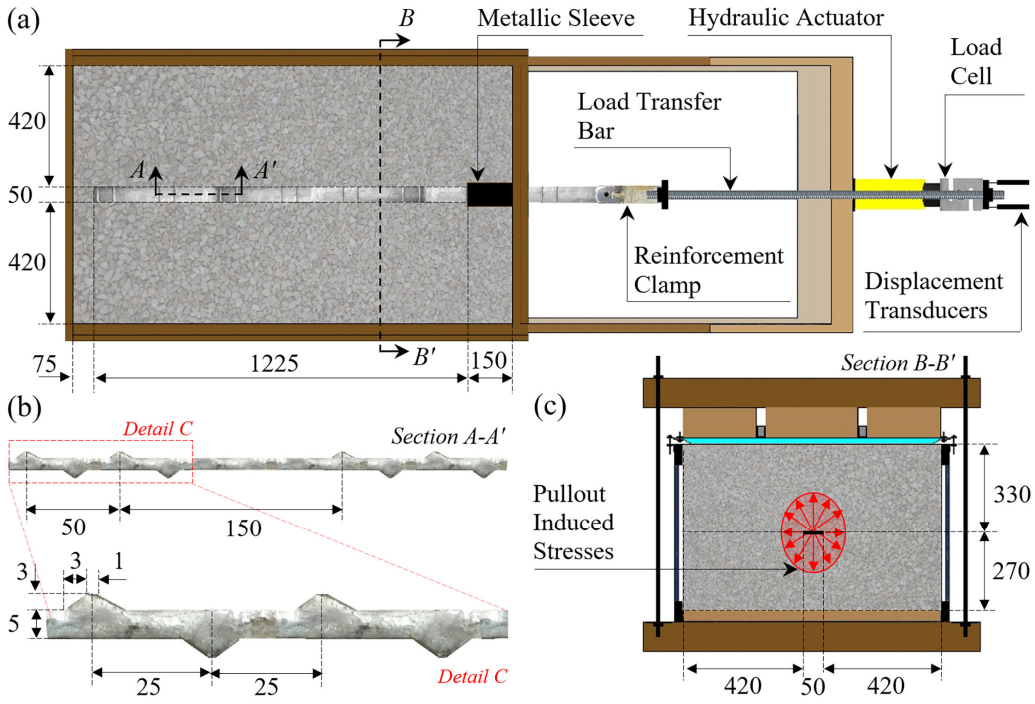

Figure 5. Pullout device details (in millimeters): (**a**) reinforcement arrangement and instrument positioning, (**b**) reinforcement geometry and dimensions of transverse ribs, and (**c**) vertical cross-section illustrating stresses induced by pullout.

Ribbed metal strips were used as reinforcement elements, which are commonly employed in MSE walls due to the corrosion resistance provided by galvanized steel. The strips had a width of 50 mm and were installed with an anchorage length of 1225 mm. A cross-sectional view (A-A′) of a segment of the reinforcement element is shown in Figure 5b, along with a detail of the rib geometry. It should be noted that the ribs are arranged in pairs, with elements spaced 50 mm apart, and the pairs repeat every 150 mm on a given face of the strip. Essentially, the ribs have a trapezoidal shape, with a smaller base and a larger base of 1 mm and 7 mm, respectively, spaced 3 mm apart. The basic function of the ribs is to increase the passive resistance during the reinforcement pullout [7,8].

Figure 5c illustrates a cross-sectional view of the equipment (B-B′), indicating the reinforcement placement and pullout-induced stresses in the adjacent region. The figure also shows the system for vertical load application, which uses a rubber membrane supplied with pressurized water and can apply vertical stresses up to 50 kPa. An air–water interface system was employed to supply the vertical load application system, and dual layers of lubricating oil and polyethylene film were applied to the inner faces of the pullout box to reduce surface friction.

To attain the necessary compaction (Table 2) for RS, AS, and NS, the sand-raining technique [57] [Figure 4b] is used. It is worth noting that, in the case of sands, the exclusive use of the sand-raining technique was unable to achieve a relative density (I_d) of 95% (Table 2), necessitating additional vibration using a mechanical hammer. On the other hand, RG and LS soil were compacted solely using mechanical compaction. In contrast, RG and LS were compacted exclusively using mechanical compaction. These techniques

were applied in 90 mm-thick layers, using soils with a moisture content matching the w_{target}. Calibration procedures were employed to adjust the soil compaction techniques, ensuring that the specified parameters in Table 2 were achieved. Additionally, undisturbed soil samples were extracted after the pullout tests, allowing for the verification of the soil compaction requirements.

The pullout tests were performed under unsaturated conditions with vertical stresses applied at the reinforcement level ($\sigma_{v,0}$) of 12.5, 25, and 50 kPa. To conduct the tests, the hydraulic cylinder shown in Figure 5a was utilized, which enabled a displacement rate of 1 mm/min and allowed for a maximum displacement of 100 mm at the external extremity of the reinforcement. During the tests, the pullout forces (P) and head displacements (δ_{face}) were measured. The experimental results were utilized to determine the pullout strength of the reinforcement considering each material, which is discussed in further detail below.

The interface shear resistance in pullout tests was calculated using the following equation [58]:

$$\tau_{max} = f^* \times \sigma_{v,0} \tag{2}$$

where τ_{max} is the shear resistance under failure conditions, $\sigma_{v,0}$ is the initial vertical stress, and f^* is the apparent friction coefficient.

After performing pullout tests on the reinforcement specimens, the gathered data were analyzed to evaluate the pullout strength, which is a crucial parameter in assessing the effectiveness of reinforcement systems. To establish a consistent calculation procedure, the following calculation procedure was employed for all the soils studied in this research. Specifically, the maximum pullout forces (P_{max}) and the corresponding head displacement ($\delta_{face,max}$) at failure were considered, and the values of f^* were calculated as follows:

$$f^* = \frac{P_{max}}{2 \times L_r \times W_r \times \sigma_{v,0}} \tag{3}$$

where L_r denotes the anchorage length of the reinforcement, while W_r refers to its width.

It should be noted that the initial vertical stress ($\sigma_{v,0}$) acting on the reinforcement plane is a combination of the surcharge stress from loading devices on the soil specimen's upper surface and vertical geostatic soil pressure on the reinforcement, which varies based on the degree of confinement provided by the compacted soil. Pullout testing can result in local stress increases along the reinforcement at the interface between the reinforcement and the dense, compact, dilatant fill material [59,60], as shown in Figure 5c. Thus, the actual stress level experienced by the reinforcement elements can be significantly higher than $\sigma_{v,0}$ [5], depending on their characteristics. This can have important technical implications for the MSW wall design, as discussed in subsequent sections of this article.

Furthermore, based on the pullout tests, a study was conducted regarding the pre-peak behavior of the reinforcement. For this purpose, a hyperbolic analytical model was employed to accurately depict the correlation between normalized pullout forces and displacements [61]:

$$P_n = \frac{\delta_n}{n_1 + n_2 \times \delta_n} \tag{4}$$

where n_1 and n_2 represent thet dimensionless coefficients of the model, in addition to the normalized pullout force (P_n) and normalized head displacement (δ_n).

In Equation (4), P_n and δ_n are defined as P/P_{max} and $\delta_{face}/\delta_{face,max}$, respectively. Here, P and δ denote the values of the pullout force and head displacement at a specific moment during the reinforcement pullout, prior to reaching peak conditions.

4. Results and Discussion

The test results are presented and discussed in this section, followed by an analytical approach based on the collected information.

4.1. Load-Displacement Behavior

Figure 6 illustrates the load-displacement curves obtained from the pullout tests, indicating the maximum pullout loading and the corresponding head displacement (P_{max} and $\delta_{face,max}$, respectively) where the failure condition occurred. Based on these results, f^* values were calculated using Equation (3) and are presented in Table 3.

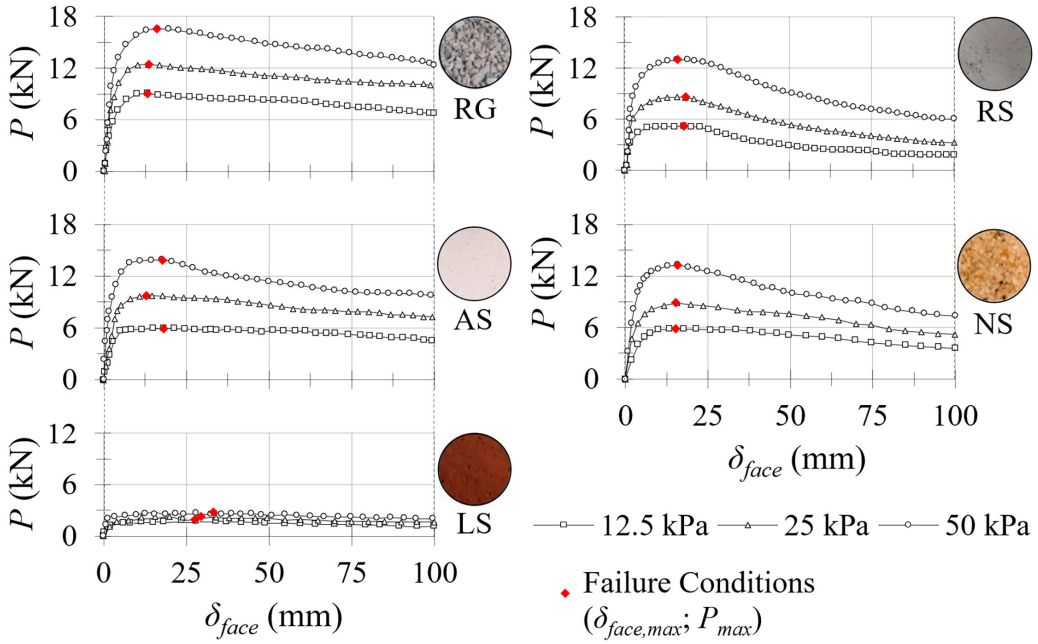

Figure 6. Pullout test results in terms of forces (P) and head displacements (δ_{face}), highlighting the failure conditions (maximum pullout forces, P_{max}, and their corresponding head displacements, $\delta_{face,max}$).

Table 3. Summary of pullout test results.

Fill Soil	$\sigma_{v,0}$ (kPa)	P_{max} (kN)	$\delta_{face,max}$ (mm)	f^* (-)
RG	12.5	9.02	13.15	5.89
	25.0	12.41	13.50	4.06
	50.0	16.55	16.05	2.70
RS	12.5	5.23	18.02	3.42
	25.0	8.68	18.50	2.83
	50.0	13.01	15.91	2.12
AS	12.5	5.93	18.15	3.87
	25.0	9.78	12.72	3.20
	50.0	13.88	17.72	2.27
NS	12.5	5.88	15.22	3.84
	25.0	8.86	15.30	2.89
	50.0	13.24	15.91	2.16
LS	12.5	1.84	27.57	1.21
	25.0	2.29	29.43	0.75
	50.0	2.71	33.21	0.44

Table 3 presents several symbols and their meanings, including the initial vertical stress ($\sigma_{v,0}$), maximum pullout force (P_{max}), head displacement at the maximum pullout force ($\delta_{face,max}$), and the apparent friction coefficient (f^*).

The results (Figure 6 and Table 3) show that particle size had a significant impact on the outcomes, with larger aggregates demonstrating superior performance, while finer fill materials yielded progressively lower parameters as the vertical stress increased. RG exhibited higher pullout resistance values than the other tested materials, suggesting that coarse, dilatant materials could provide enhanced pullout performance compared to finer granular soils. Further investigation should be conducted to assess the potential loss of

performance in this material due to surface cracks observed through SEM analysis [see Figure 2b], as elevated stress levels may arise at the grain-to-grain contact.

AS demonstrated superior performance compared to other sands, indicating that the enhanced surface roughness and angularity of its particles, attributed to the crushing process of metamorphic rock, promoted better interlocking among the sand grains, leading to increased pullout forces. Additionally, it is noteworthy that AS benefits from the higher strength of the metamorphic rock matrix when compared to other types of aggregates, which can even mitigate potential grain breakage. On the other hand, NS showed intermediate performance between AS and RS, possibly due to the lower angularity of the natural sand grains in comparison to the artificial aggregate.

Regarding RS, a lower mobilization of resistance to pullout forces was observed compared to other types of sands. This behavior may be attributed to the surface cracks observed through SEM analysis [Figure 2c], which could have contributed to a higher level of grain breakage during the test. However, both recycled gravel and sand materials demonstrated good potential for use as fill material in MSE walls reinforced with strips, as long as additional safety coefficients are taken into consideration, encompassing the possibility of additional grain breakage when using these materials.

LS showed lower pullout resistance levels than the other tested materials. This indicates that the formation of aggregates provided by the sesquioxide coating, which have dimensions similar to natural sands and occur in the field when the lateritic soil is present, does not translate into a dilatant behavior that would be expected from sands with similar particle sizes. This factor may be related to the relatively high fines content (F_c) values of 0.648 and 0.314 (Table 1), considering tests with and without the use of a dispersing agent (DA), respectively, which could have inhibited the dilatant behavior of this soil type. Moreover, this behavior aligns with the plasticity exhibited by LS, with w_L and w_P values of 0.39 and 0.28, respectively, contrary to the other soils used in the study.

In terms of the practical applications of LS in earthworks, it should be noted that previous investigations described in the technical literature have indicated that this material performs well as a compacted base and sub-base in road structures [30,34]. However, this behavior, which is considered adequate for pavement applications, did not result in a favorable performance in terms of MSE walls reinforced with strips, as LS was unable to mobilize pullout resistance compatible with those of non-cohesive fill materials. This result is consistent with a previous study that employed polymeric strips embedded in sand–silt mixtures [5].

In order to conduct a more in-depth analysis, the present study developed the following analytical approach to precisely illustrate the non-linear correlation between P_{max} and $\sigma_{v,0}$:

$$P_{max} = m \times \sqrt{\sigma_{v,0} \times p_a \times A_r^2} \quad (5)$$

where m represents a dimensionless model coefficient; p_a denotes the atmospheric pressure, which has a constant value of 101 kPa; and A_r represents the reinforcement surface area of a single side, which can be calculated as the product between the length (L_r) and width (W_r) of the reinforcement.

Equation (5) was developed using mathematical modeling software, which enabled the establishment of the best approach for correlating the variables P_{max} and $\sigma_{v,0}$. The inclusion of the values p_a and A_r in the model was necessary to adjust the units of measurement, as the coefficient m is dimensionless. The values obtained using Equation (5) are applicable for a range of $0 < \sigma_{v,0} \leq 50$ kPa, with a high level of statistical agreement ($R^2 > 0.94$) observed for each set of data points. Table 4 summarizes the values of the dimensionless model coefficient, along with other analytical parameters assessed in this study.

Table 4. Analytical approximations and corresponding fitted variables used to represent experimental results.

Equation	y = Function (x)	x	Valid Domain	Fill Soil	Fitted Coefficients	R^2 (-)
(5)	P_{max} (kN)	$\sigma_{v,0}$ (kPa)	$0 < \sigma_{v,0} \leq 50$ kPa	RG	m, 3.9181	0.9958
(5)	P_{max} (kN)	$\sigma_{v,0}$ (kPa)	$0 < \sigma_{v,0} \leq 50$ kPa	RS	m, 2.8576	0.9855
(5)	P_{max} (kN)	$\sigma_{v,0}$ (kPa)	$0 < \sigma_{v,0} \leq 50$ kPa	AS	m, 3.1204	0.9918
(5)	P_{max} (kN)	$\sigma_{v,0}$ (kPa)	$0 < \sigma_{v,0} \leq 50$ kPa	NS	m, 2.9466	0.9947
(5)	P_{max} (kN)	$\sigma_{v,0}$ (kPa)	$0 < \sigma_{v,0} \leq 50$ kPa	LS	m, 0.6905	0.9457
(4)	P_n (-)	δ_n (-)	$0 < \delta_n \leq 1$	RG	n_1, 0.1406; n_2, 0.8115	0.9881
(4)	P_n (-)	δ_n (-)	$0 < \delta_n \leq 1$	RS	n_1, 0.1356; n_2, 0.7998	0.9220
(4)	P_n (-)	δ_n (-)	$0 < \delta_n \leq 1$	AS	n_1, 0.1069; n_2, 0.8480	0.9355
(4)	P_n (-)	δ_n (-)	$0 < \delta_n \leq 1$	NS	n_1, 0.1410; n_2, 0.8214	0.9740
(4)	P_n (-)	δ_n (-)	$0 < \delta_n \leq 1$	LS	n_1, 0.0271; n_2, 1.0163	0.9356

In Table 4, y denotes the independent variables [i.e., y = function (x)] while x represents the dependent variables. The symbols indicated in Table 4 are the following: maximum pullout force (P_{max}), normalized pullout force (P_n), initial vertical stress ($\sigma_{v,0}$), coefficient used in Equation (5) (m), coefficients used in Equation (4) (n_1, n_2), and normalized head displacement (δ_n).

The results of the nonlinear fitting between the normalized pullout force (P_n) and the normalized head displacement (δ_n) are presented in Table 4, following the calculation procedures based on Equation (4). By restricting the range to $0 < \delta_n \leq 1$, a strong statistical agreement ($R^2 > 0.90$) with the experimental data was achieved.

Figure 7 provides a graphical representation of the analytical results, with Figure 7a depicting the pullout force variation with initial vertical stress and Figure 7b illustrating the pullout force mobilization prior to reaching the peak conditions.

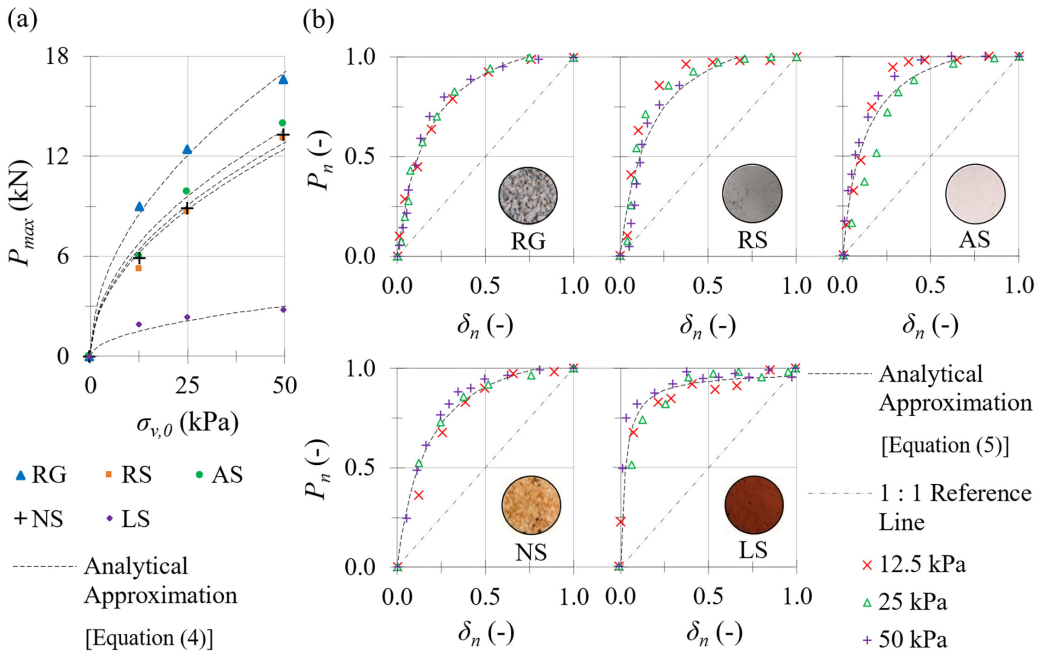

Figure 7. Variables related to ribbed metal strips pullout: (**a**) analytical envelopes showing the correlation between maximum pullout loads (P_{max}) and initial stress conditions ($\sigma_{v,0}$), and (**b**) hyperbolic function describing the progressive mobilization of reinforcement in terms of loads and displacements in the pre-peak segment.

Figure 7a reveals that the type of backfill material significantly impacts the mobilization of pullout resistance. For instance, RG displayed relatively superior behavior compared to the other samples, while similar results were observed for the sands (RS, AS, and NS) due to the similarity in their particle size distributions. In contrast, the envelope

corresponding to LS indicates considerably lower values than the other materials, consistent with the previous discussion.

The results presented in Figure 7b demonstrate that a significant portion of P_{max} is mobilized with relatively small increases in head displacement, as evidenced by the curves relating P_n and δ_n deviating significantly from the 1:1 reference line representing proportional mobilization. Minor variations were observed among different materials. Overall, these findings indicate that the presence of ribs in the metal strips results in a considerable portion of the maximum load being mobilized early in the pullout process. This differs from synthetic elements, as discussed in [5,61], where a delayed mobilization of pullout forces was observed.

Figure 8 provides a comparison between $\delta_{face,max}$ and P_{max} at failure conditions for different backfill materials to better understand their impact on pullout responses. Specifically, Figure 8a presents the results in terms of $\delta_{face,max}$, while Figure 8b displays the corresponding P_{max} values.

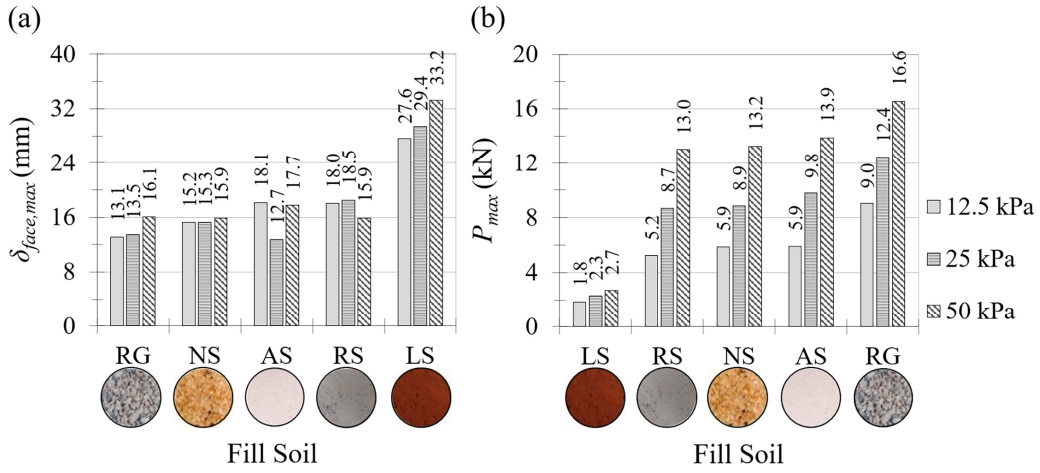

Figure 8. Comparison of pullout responses at failure conditions: (**a**) head displacements at maximum pullout forces ($\delta_{face,max}$), and (**b**) maximum pullout forces (P_{max}).

Regarding $\delta_{face,max}$ [Figure 8a], it is clear that RG exhibited lower displacement levels than the other tested materials, which was expected as gravelly fills tend to mobilize greater resistance at early stages of pullout than materials with smaller particle sizes. NS mobilized larger face displacements than RG but smaller than the other sands (AS and RS), which behaved similarly. Finally, LS exhibited the worst performance in terms of the level of displacement required to reach maximum loading, raising concerns about the effectiveness of using this material as backfill in MSE walls due to the possibility of greater external wall displacements.

When analyzing P_{max} [Figure 8b], it is evident that LS mobilized the lowest pullout forces compared to the other soils, once again indicating that the presence of aggregates with particle sizes similar to sands did not provide it with a performance comparable to that of sands under field conditions. The sands (RS, NS, and AS) exhibited similar behavior, with a slight trend of higher force mobilization in the case of NS and AS, respectively, compared to RS. Finally, RG showed higher pullout resistances compared to the other materials, which is consistent with the larger sizes of these aggregates and their enhanced geomechanical properties compared to those of the other soils.

4.2. Conventional Methods for Pullout Resistance Prediction

The purpose of this section is to evaluate the adequacy of conventional methods for predicting the design variables of MSE walls reinforced with ribbed strips, namely, the apparent pullout friction coefficients (f^*), and to propose an alternative method for

incorporating variables related to the specific characteristics of the soils studied in this research into f^* prediction procedures.

The first design approach evaluated in this research was the one proposed by the American Association of State Highway and Transportation Officials (AASHTO) [62], which suggests that the value of f^* can be estimated using the following bilinear function:

$$f^* = f_0 \times \left(1 - \frac{z}{z_0}\right) + f_1 \times \left(\frac{z}{z_0}\right), \text{ for } z \leq z_0, \quad (6)$$

$$f^* = f_1, \text{ for } z > z_0, \quad (7)$$

where z represents the installation depth, which was calculated as $\sigma_{v,0}/\gamma_{b,target}$ in this study; z_0 denotes the break-point depth assumed to be 6 m; and f_0 and f_1 are, respectively, the maximum and minimum values of f^* allowed in the design.

The design approach proposed by [62] suggests that, in the absence of less conservative data, f_0 can be estimated using the relationship 1.2 + log C_u, with this value limited to 2.0, while f_1 can be calculated as tan ϕ_s, where ϕ_s is the soil friction angle. Alternatively, values proposed by [63,64], which are valid for sandy fill soils, and values proposed by [65], which encompasses gravelly fill soils, were also considered. It should be noted that the values suggested by the last three authors were established based on a statistical analysis considering several pullout tests conducted on ribbed metallic strips. Figure 9 presents comparisons between the experimental and predicted results as a function of the depth in a hypothetical MSE wall, with z equal to the ratio between vertical stress and soil unit weight.

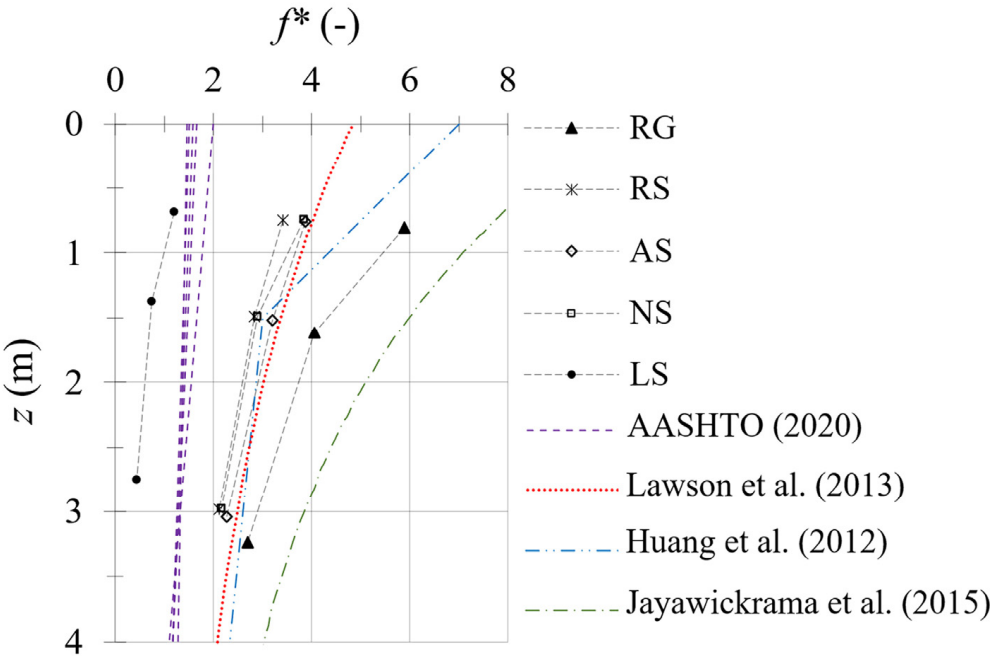

Figure 9. Comparison of laboratory-obtained apparent friction coefficients (f^*) with analytical predictions from different sources, including sandy fill soils [63,64], gravelly fill soils [65], and a combination of both [62].

Based on the results presented in Figure 9, it can be observed that the predicted f^* values, according to [62], are considerably lower than the experimentally obtained results for RG, RS, AS, and NS, while the estimated results for LS greatly exceeded the experimental values of f^*. It is important to note that the AASHTO formulation [62] was designed considering a wide range of soils and different testing conditions, to which a statistical envelope was implemented to represent several situations. Therefore, when considering high-quality fill materials, the results found may be considered conservative.

On the other hand, in the case of low-quality soils (such as the LS used in this study), the assumed values of f^* may be overestimated, posing a safety risk.

According to Figure 9, the methods proposed by [63,64] were able to predict the experimental f^* values for sands (RS, AS, and NS) with reasonable accuracy. Specifically, when comparing the actual and predicted values of f^* for the tested depths, R^2 values higher than 0.95 were obtained for the method proposed by [63], while this value was higher than 0.80 for the method proposed by [64]. The difference is due to the better fit between the experimental results and the method proposed by [63] when it comes to shallow depths. It is important to note that, despite the distinct origins of the sands used in the study and the small performance differences between different types of sands, the particle size distribution of these soils was a conditioning factor in mobilizing forces during reinforcement pullout.

Morever, considering the data presented in Figure 9, the f^* values proposed by [65], considering gravelly materials as fill in MSE walls, overestimate the experimental results for RG. This could be due to the breakage of larger aggregates [25,43,44] during pullout, as the stresses mobilized may exceed the stresses initially applied to the reinforcement, as schematically shown in Figure 5c. This behavior may be more pronounced due to the use of CDW aggregate and the relatively large dimensions of the gravelly fill, which exacerbate stress concentrations at the contacts between the gravel particles. Moreover, it should be noted that the CDW recycled aggregates (namely, RG and RS) have a considerable portion of calcite (12.9%) in their mineralogical composition [Figure 1b], which may facilitate grain breakage along cleavage planes. Further investigations should be carried out to quantify the potential effect of particle breakage on the reduction of pullout resistance in gravelly fills in MSE walls. Nevertheless, it is observed that the larger dimensions of the gravely fill led to higher f^* values compared to sands.

4.3. Improved Predictive Model

An alternative method is proposed herein for predicting the pullout responses of ribbed metallic strips installed in soils with varying geotechnical properties based on the particle size distribution, given the relevance of this parameter in the pullout responses, as observed in the previous section. It is important to note that the proposed method consists of a preliminary design approach that can facilitate decision making in early stages of the project when there is limited knowledge about the soil–reinforcement interface behavior, but the particle size distribution is known. The method relies on the nonlinear relationship between P_{max} and $\sigma_{v,0}$, as expressed in Equation (5), which is dependent on a dimensionless coefficient, m. Several attempts were made to correlate m with the geotechnical properties of the soil. It was observed that the best correlation was achieved in terms of particle size distribution attributes. Specifically, the pre-dimensioning method assumes the calculation of a dimensionless coefficient related to the soil size distribution, which can be established as follows:

$$C_d = \frac{C_u}{C_c} = \frac{D_{60}^2}{D_{30}^2}, \tag{8}$$

where C_d is the soil size distribution coefficient, C_u represents the non-uniformity coefficient, C_c represents the curvature coefficient, and D_{30} and D_{60} represent the soil diameters corresponding to 30% and 60% passing, respectively.

The implementation of the C_d parameter in the model was particularly interesting as the C_u and C_c parameters can be easily determined based on the particle size distribution curve. Regarding this last test, it is worth noting that, as stated in [48], it is necessary to perform a hydrometer analysis for soils containing more than approximately 5% of fine-grained material, where the fine fraction is defined as particles with diameters smaller than 0.075 mm. This consideration was maintained in this research. However, for the lateritic soil subject to particle aggregation, the dimensions to be considered in the calculation of the C_d parameter were those corresponding to the hydrometer test with no solution stirring

and dispersing agent (DA), as per [49]. In other words, the dimensions of the aggregates were considered instead of those of individual soil particles.

After estimating the C_d parameter for each soil, a linear regression was performed between the experimentally obtained values of m (Table 4) and C_d. This allowed for the empirical adjustment of the dimensionless coefficient m, corresponding to Equation (5), based on the following experimentally obtained relationship:

$$m = 4.9307 - 0.8154 \times C_d, \quad (9)$$

where m is a dimensionless coefficient associated with the pullout of ribbed metallic strips in soils with different particle dimensions.

By considering the calculated value for the parameter m, the maximum pullout loads (P_{max}) can be predicted using Equation (5). Subsequently, the parameter P_{max} serves as an input argument in the calculation of the variable f^* using Equation (3). In summary, the input variables of the model are C_u and C_c, which allow us to estimate a value for m, which, in turn, estimates the values of P_{max} and f^* for different values of $\sigma_{v,0}$.

As an example of application, Figure 10 provides a comparison between experimental values of C_d and m, and the analytical envelope implemented on the dataset, along with corresponding lower and upper 95% confidence bounds [Figure 10a]. Next, the distribution of the estimated values of f^* along the depth is presented [Figure 10b], along with a comparison between the values obtained from laboratory tests and those predicted using the method described in this study [Figure 10c].

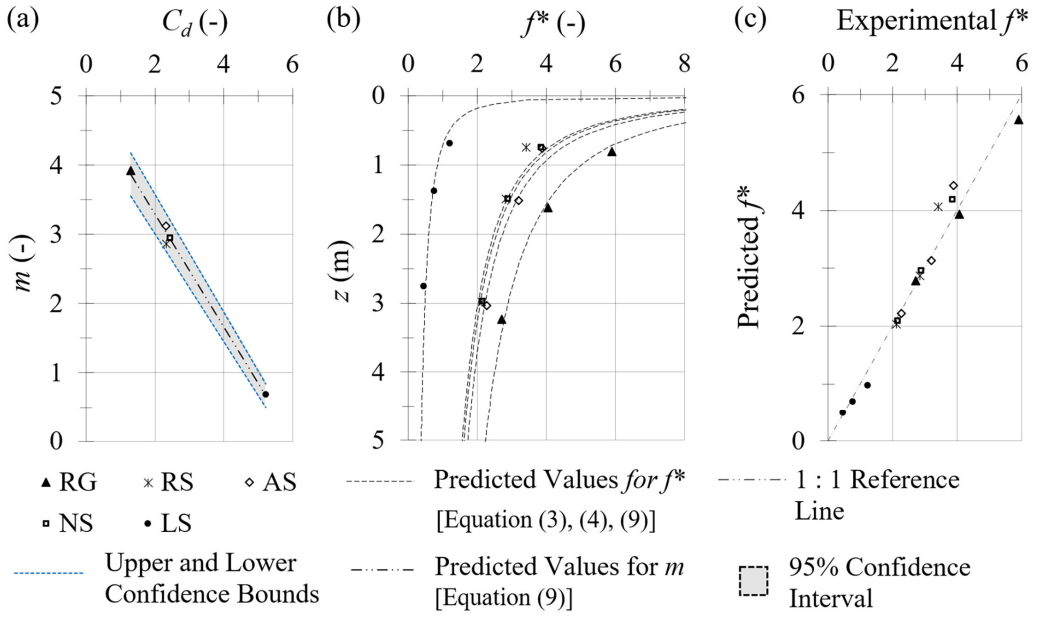

Figure 10. Predictive model for pullout resistance: (**a**) calibration of the dimensionless model variable (m), (**b**) predicted values of f^* over depth, and (**c**) comparison between experimental and predicted values of f^*, considering $\sigma_{v,0}$ of 12.5, 25, and 50 kPa.

Based on Figure 10a, it can be observed that the predicted values of m (dashed line) closely matched the experimental values for all soil types. Thus, it is considered that the C_d parameter, used as an input variable in the model, effectively represented the behavior of the different soil types employed in the study. Furthermore, the proposed model was effective in providing insight into the values assumed by f^* along the depth [Figure 10b], which is particularly useful for the design of MSE walls reinforced with strips. The proximity between the experimental and predicted values of f^* [Figure 10c] for all soil types is also an indication of the feasibility of using the proposed model.

One of the main advantages of this method is its simplicity, as it relies on particle dimension attributes (C_u and C_c) which are generally determined in the early stages of the project and are used to calculate the parameter C_d. Additionally, the results showed that the consideration of C_d in predicting f^* was able to detect nuances in the behavior of alternative fill materials used in the study, ranging from gravel to fine soils with lateritic behavior. Finally, the resulting nonlinear distribution of f^* with depth is crucial for designing mechanically stabilized earth (MSE) walls, however, is often not considered in traditional design guidelines. Further research is necessary to expand the applicability of the proposed method to other types of soils and reinforcements.

5. Conclusions

The aim of this study was to investigate the potential use of alternative fill materials in mechanically stabilized earth (MSE) walls, by conducting large-scale pullout tests on ribbed metallic strips embedded in various types of fill soils. These fill soils included gravelly and sandy recycled aggregates from construction and demolition waste (CDW), as well as sandy and silty materials obtained from natural deposits, and an artificial sand. The main findings of the study are as follows:

- CDW aggregates can replace natural ones in constructing MSE walls. Recycled sand (RS) from CDW has similar properties to natural and artificial sands (NS and AS, respectively); however, additional research is needed to assess particle crushing in recycled gravel (RG) during pullout tests, as well as potential environmental contamination caused by CDW.
- The chemical and mineral composition of fill soils affects their geomechanical properties. The silica–sesquioxides ratio (*SSR*) parameter reflects the proportion of stable minerals to weathering products. The lateritic soil (LS) had a lower *SSR* value than the granular materials (RG, RS, AS, and NS), resulting in significant variations in pullout responses compared to other samples.
- LS showed lower pullout resistance levels than the other tested materials, indicating that the formation of aggregates provided by the sesquioxide coating does not translate into a dilatant behavior that would be expected of sands with similar particle size.
- A new analytical approach has been proposed to accurately capture the pre-peak behavior of reinforcement pullout, based on the non-linear correlation between the apparent friction coefficients (f^*) and depth. This approach was found to have a high level of agreement with testing results and could offer an expedited alternative for predicting pullout strength based on particle size for pre-design purposes.

The study results suggest that the use of alternative fill materials in MSE walls could be a cost-effective and environmentally friendly solution. The findings of this study have important implications for the design and performance assessment of MSE walls and provide a useful tool for engineers and researchers working in this field. Specifically, this study contributes to the design and construction of MSE walls reinforced with strips by facilitating estimations of the behavior of poor fill soils based on the particle size distribution of the material, particularly during the preliminary design stages. As a result, this study contributes to sustainability by providing insights for engineers to consider the use of poor backfill materials in construction projects. These materials can exhibit behavior comparable to conventional aggregates while reducing the need for the extraction of the latter, thus offering potential economic, social, and environmental benefits.

However, it is important to note that the unique characteristics of these poor backfill materials have not been fully considered in the currently available design guidance, and further investigation is required from a technical standpoint to identify potential incompatibilities of these materials. Future research should consider assessing the geomechanical behavior of soil mixtures by evaluating combinations of different soils. This would help in enhancing their overall performance and characteristics.

Author Contributions: Conceptualization, L.A.G.C., R.C.P. and G.L.S.A.; methodology, L.A.G.C. and R.C.P.; software, L.A.G.C.; validation, L.A.G.C., R.C.P., G.L.S.A. and E.M.P.; formal analysis, L.A.G.C. and R.C.P.; investigation, L.A.G.C., R.C.P., G.L.S.A. and E.M.P.; resources, G.L.S.A. and E.M.P.; data curation, L.A.G.C., R.C.P., G.L.S.A. and E.M.P.; writing—original draft preparation, L.A.G.C. and R.C.P.; writing—review and editing, L.A.G.C. and R.C.P.; visualization, L.A.G.C. and R.C.P.; supervision, G.L.S.A. and E.M.P.; project administration, G.L.S.A. and E.M.P.; funding acquisition, G.L.S.A. and E.M.P. All authors have read and agreed to the published version of the manuscript.

Funding: The research was funded by the University of Brasilia, the Co-ordination for the Improvement of Higher Education Personnel (CAPES), the National Council for Scientific and Technological Development (CNPq), and the Federal District Research Foundation (FAP-DF), which includes research projects number 407293/2018-3 (CNPq) and 00193-00000133/2019-48 (FAP-DF). Additionally, the first author received research funding provided by the University of Costa Rica (UCR) and the Office of International Affairs and External Co-operation (OAICE).

Institutional Review Board Statement: Not applicable.

Informed Consent Statement: Not applicable.

Data Availability Statement: Data will be provided upon request.

Acknowledgments: The authors would like to express their gratitude to the University of Brasília, the Co-ordination for the Improvement of Higher Education Personnel (CAPES), the National Council for Scientific and Technological Development (CNPq), and the Federal District Research Foundation (FAP-DF) for their generous funding and support of this research, which includes research projects number 407293/2018-3 (CNPq) and 00193-00000133/2019-48 (FAP-DF). Additionally, the first author would like to extend his appreciation to the University of Costa Rica (UCR) and the Office of International Affairs and External Co-operation (OAICE) for funding and supporting his research activities.

Conflicts of Interest: The authors declare no conflict of interest.

Abbreviations

AASHTO—American Association of State Highway and Transportation Officials; AS—Artificial sand; BSI—British Standard Institution; CDW—Construction and demolition waste; DA—Dispersing agent; FHWA—Federal Highway Administration; GP—Poorly graded gravel; LS—Lateritic soil; ML—Low-plasticity silt; MSE—Mechanically stabilized earth; NCMA—National Concrete Masonry Association; NS—Natural sand; RG—Recycled gravel; RS—Recycled sand; SEM—Scanning Electron Microscopy; SP—Poorly graded sand; SM—Silty sand; USCS—Unified Soil Classification System; XRD—X-Ray Diffraction; XRF—X-Ray Fluorescence. **Symbols:** $\gamma_{d:max}$—Maximum dry unit weight (kN/m^3); $\gamma_{b,target}$—Target bulk unit weight of soil (kN/m^3); $\gamma_{d,target}$—Target dry unit weight of soil (kN/m^3); δ_{face}—Head displacement (mm); $\delta_{face,max}$—Head displacement associated with the maximum pullout force (mm); δ_n—Normalized head displacement; $\sigma_{v,0}$—Initial vertical stress (kPa); ϕ_s—Soil friction angle (degrees); A—Value attributed to the $\%Al_2O_3/102$ relation in Equation (1); A_r—Reinforcement surface area of a single side (m^2); C_c—Coefficient of curvature; C_d—Soil size distribution coefficient; c_s—Cohesion intercept of the soil shear resistance (kPa); C_u—Coefficient of non-uniformity; D—Particle diameter (mm); D_{10}—Diameter corresponding to 10% passing soil (mm); D_{30}—Diameter corresponding to 30% passing soil (mm); D_{50}—Diameter corresponding to 50% passing soil (mm); D_{60}—Diameter corresponding to 60% passing soil (mm); D_c—Degree of compaction; e_{max}—Maximum void ratio; e_{min}—Minimum void ratio; e_{target}—Target void ratio of soil; f^*—Apparent friction coefficient; F—Value attributed to the $\%Fe_2O_3/160$ relation in Equation (1); F_c—Fines content (the mass fraction with a diameter smaller than 0.075 mm); G_s—Specific gravity of solids; I_d—Relative density; LA—Los Angeles abrasion index; L_r—Reinforcement length (m); m—Coefficient used in Equation (5); n_1, n_2—Coefficients used in Equation (4); P—Pullout force (kN); p_a—Atmospheric pressure (kPa); PI—Plasticity index; P_{max}—Maximum pullout force (kN); P_n—Normalized pullout force; R^2—Coefficient of determination; S—Value attributed to the $\%SiO_2/60$ relation in Equation (1); SSR—Silica–sesquioxides ratio; w_L—Liquid limit; w_{opt}—Optimum water content; w_P—Plastic limit; W_r—Reinforcement width (m); w_{target}—Target water content of soil.

References

1. Strahler, A.W.; Walters, J.J.; Stuedlein, A.W. Frictional Resistance of Closely Spaced Steel Reinforcement Strips Used in MSE Walls. *J. Geotech. Geoenviron.* **2016**, *142*, 04016030. [CrossRef]
2. Benmebarek, S.; Attallaoui, S.; Benmebarek, N. Interaction analysis of back-to-back mechanically stabilized earth walls. *J. Rock Mech. Geotech. Eng.* **2016**, *8*, 697–702. [CrossRef]
3. Koerner, R.M.; Koerner, G.R. An extended data base and recommendations regarding 320 failed geosynthetic reinforced mechanically stabilized earth (MSE) walls. *Geotext. Geomembr* **2018**, *46*, 904–912. [CrossRef]
4. Mirzaeifar, H.; Hatami, K.; Abdi, M.R. Pullout testing and Particle Image Velocimetry (PIV) analysis of geogrid reinforcement embedded in granular drainage layers. *Geotext. Geomembr.* **2022**, *50*, 1083–1109. [CrossRef]
5. Pierozan, R.C.; Araujo, G.L.S.; Palmeira, E.M.; Romanel, C.; Zornberg, J.G. Interface pullout resistance of polymeric strips embedded in marginal tropical soils. *Geotext. Geomembr.* **2022**, *50*, 20–39. [CrossRef]
6. Ijaz, N.; Dai, F.; Rehman, Z.U. Paper and wood industry waste as a sustainable solution for environmental vulnerabilities of expansive soil: A novel approach. *J. Environ. Manag.* **2020**, *262*, 110285. [CrossRef]
7. Elias, V.; Christopher, B.R.; Berg, R.R. *Mechanically Stabilized Earth Walls and Reinforced Soil Slopes Design and Construction Guidelines*, 1st ed.; U.S. Department of Transportation: Washington, DC, USA, 2001; pp. 1–394.
8. Berg, R.R.; Christopher, B.R.; Samtani, N.C. *Design and Construction of Mechanically Stabilized Earth Walls and Reinforced Soil Slopes, Volume I*; U.S. Department of Transportation: Washington, DC, USA, 2009; pp. 1–332.
9. Berg, R.R.; Christopher, B.R.; Samtani, N.C. *Design and Construction of Mechanically Stabilized Earth Walls and Reinforced Soil Slopes, Volume II*; U.S. Department of Transportation: Washington, DC, USA, 2009; pp. 1–404.
10. *NF P94-270*; Geotechnical Design–Retaining Structures–Reinforced and Soil Nailing Structures (in French). 1st ed. Association Française de Normalisation: Paris, France, 2009; pp. 1–205.
11. *BS 8006-1*; Code of Practice for Strengthened/Reinforced Soils and Other Fills (+A1:2016). 1st ed. British Standards Institution: Chiswick, UK, 2010; pp. 1–250. [CrossRef]
12. *TR 127B*; Design Manual for Segmental Retaining Walls. 5th ed. National Concrete Masonry Association: Herndon, VA, USA, 2012; pp. 1–284.
13. Zhang, H.; Yuan, X.; Liu, Y.; Wu, J.; Song, X.; He, F. Experimental study on the pullout behavior of scrap tire strips and their application as soil reinforcement. *Constr. Build Mater.* **2020**, *254*, 119288. [CrossRef]
14. Santos, E.C.G.; Palmeira, E.M.; Bathurst, R.J. Behaviour of a geogrid reinforced wall built with recycled construction and demolition waste backfill on a collapsible foundation. *Geotext. Geomembr.* **2013**, *39*, 9–19. [CrossRef]
15. Santos, E.C.G.; Palmeira, E.M.; Bathurst, R.J. Performance of two geosynthetic reinforced walls with recycled construction waste backfill and constructed on a collapsible ground. *Geosynth. Int.* **2014**, *21*, 256–269. [CrossRef]
16. Beja, I.A.; Motta, R.; Bernucci, L.B. Application of recycled aggregates from construction and demolition waste with Portland cement and hydrated lime as pavement subbase in Brazil. *Constr. Build. Mater.* **2020**, *258*, 119520. [CrossRef]
17. Vieira, C.S.; Pereira, P.; Ferreira, F.; Lopes, M.d.L. Pullout Behaviour of Geogrids Embedded in a Recycled Construction and Demolition Material. Effects of Specimen Size and Displacement Rate. *Sustainability* **2020**, *12*, 3825. [CrossRef]
18. Bagriacik, B. Utilization of alkali-activated construction demolition waste for sandy soil improvement with large-scale laboratory experiments. *Constr. Build. Mater.* **2021**, *302*, 124173. [CrossRef]
19. Naeini, M.; Mohammadinia, A.; Arulrajah, A.; Horpibulsuk, S. Stress-dilatancy responses of recovered plastics and demolition waste blends as a construction material. *Constr. Build. Mater.* **2021**, *297*, 123762. [CrossRef]
20. Vieira, C.S.; Pereira, P.M. Short-term tensile behaviour of three geosynthetics after exposure to Recycled Construction and Demolition materials. *Constr. Build. Mater.* **2021**, *273*, 122031. [CrossRef]
21. Vieira, C.S.; Pereira, P.M. Influence of the Goesynthetic Type and Compaction Conditions on the Pullout Behaviour of Geosynthetics Embedded in Recycled Construction and Demolition Materials. *Sustainability* **2022**, *14*, 1207. [CrossRef]
22. Paula Junior, A.C.; Jacinto, C.; Turco, C.; Fernandes, J.; Teixeira, E.; Mateus, R. Analysis of the effect of incorporating construction and demolition waste on the environmental and mechanical performance of earth-based mixtures. *Constr. Build. Mater.* **2022**, *330*, 127244. [CrossRef]
23. Pereira, P.M.; Vieira, C.S. A Literature Review on the Use of Recycled Construction and Demolition Materials in Unbound Pavement Applications. *Sustainability* **2022**, *14*, 13918. [CrossRef]
24. Malazdrewicz, S.; Ostrowski, K.A.; Sadowski, Ł. Self-compacting concrete with recycled coarse aggregates from concrete construction and demolition waste–Current state-of-the-art and perspectives. *Constr. Build. Mater.* **2023**, *370*, 130702. [CrossRef]
25. Agarwal, A.; Ramana, G.V.; Datta, M.; Soni, N.K.; Satyakam, R. Pullout behaviour of polymeric strips embedded in mixed recycled aggregate (MRA) from construction & demolition (C&D) waste–Effect of type of fill and compaction. *Geotext. Geomembr.* **2023**, *51*, 405–417. [CrossRef]
26. Ibrahim, M.; Alimi, W.; Assaggaf, R.; Salami, B.A.; Oladapo, E.A. An overview of factors influencing the properties of concrete incorporating construction and demolition wastes. *Constr. Build. Mater.* **2023**, *367*, 130307. [CrossRef]
27. Abarca-Guerrero, L.; Lobo-Ugalde, S.; Méndez-Carpio, N.; Rodríguez-Leandro, R.; Rudin-Veja, V. Zero Waste Systems: Barriers and Measures to Recycling of Construction and Demolition Waste. *Sustainability* **2022**, *14*, 15265. [CrossRef]
28. Bordoloi, S.; Afolayan, O.D.; Ng, C.W.W. Feasibility of construction demolition waste for unexplored geotechnical and geo-environmental applications- a review. *Constr. Build. Mater.* **2022**, *256*, 129230. [CrossRef]

29. Gidigasu, M.D. Mode of formation and geotechnical characteristics of laterite materials of Ghana in relation to soil forming factors. *Eng. Geol.* **1972**, *6*, 79–150. [CrossRef]
30. Araujo, G.L.S.; Moreno, J.A.S.; Zornberg, J.G. Shear behavior of mixtures involving tropical soils and tire shreds. *Constr. Build. Mater.* **2021**, *276*, 122061. [CrossRef]
31. Kaze, R.C.; Naghizadeh, A.; Tchadjie, L.; Adesina, A.; Djobo, J.N.Y.; Nemaleu, J.G.D.; Kamseu, E.; Melo, U.C.; Tayeh, B.A. Lateritic soils based geopolymer materials: A review. *Constr. Build. Mater.* **2022**, *344*, 128157. [CrossRef]
32. Mahalinga-Iyer, U.; Williams, D.J. Consolidation and shear strength properties of a lateritic soil. *Eng. Geol.* **1994**, *38*, 53–63. [CrossRef]
33. Ng, C.W.W.; Akinniyi, D.B.; Zhou, C.; Chiu, C.F. Comparisons of weathered lateritic, granitic and volcanic soils: Compressibility and shear strength. *Eng. Geol.* **2019**, *249*, 235–240. [CrossRef]
34. De Carvalho, J.C.; de Rezende, L.R.; da F. Cardoso, F.B.; de F.L. Lucena, L.C.; Guimarães, R.C.; Valencia, Y.G. Tropical soils for Highway construction: Peculiarities and considerations. *Transp. Geotech.* **2015**, *5*, 3–19. [CrossRef]
35. Etim, R.K.; Ekpo, D.U.; Attah, I.C.; Onyelowe, K.C. Effect of micro sized quarry dust particle on the compaction and strength properties of cement stabilized lateritic soil. *Clean. Mater.* **2021**, *2*, 100023. [CrossRef]
36. Tesanasin, T.; Suksiripattanapong, C.; Duc, B.V.; Tabyang, W.; Phetchuay, C.; Phoo-ngernkham, T.; Sukontasukkul, P.; Chindaprasirt, P. Engineering properties of marginal lateritic soil stabilized with one-part high calcium fly ash geopolymer as pavement materials. *Case Stud. Constr. Mater.* **2022**, *17*, e01328. [CrossRef]
37. Tran, N.Q.; Hoy, M.; Suddeepong, A.; Horpibulsuk, S.; Kantathum, K.; Arulrajah, A. Improved mechanical and microstructure of cement-stabilized lateritic soil using recycled materials replacement and natural rubber latex for pavement applications. *Constr. Build. Mater.* **2022**, *347*, 128547. [CrossRef]
38. Hoy, M.; Tran, N.Q.; Suddeepong, A.; Horpibulsuk, S.; Mobkrathok, M.; Chinkulkijniwat, A.; Arulrajah, A. Improved fatigue properties of cement-stabilized recycled materials—Lateritic soil using natural rubber latex for sustainable pavement applications. *Transp. Geotech.* **2023**, *40*, 100959. [CrossRef]
39. Sukmak, K.; Sukmak, P.; Horpibulsuk, S.; Chinkulkijniwat, A.; Arulrajah, A.; Shen, S.-L. Pullout resistance of bearing reinforcement embedded in marginal lateritic soil at molding water contents. *Geotext. Geomembr.* **2016**, *44*, 475–483. [CrossRef]
40. Chen, Y.; Gao, Y.; Yang, S.; Zhang, F. Required unfactored geosynthetic strength of three-dimensional reinforced soil structures comprised of cohesive backfills. *Geotext. Geomembr.* **2018**, *46*, 860–868. [CrossRef]
41. Ghazavi, M.; Bavandpouri, O. Analytical solution for calculation of pull out force-deformation of geosynthetics reinforcing unsaturated soils. *Geotext. Geomembr.* **2022**, *50*, 357–369. [CrossRef]
42. Catt, J.A. Tropical residual soils. Geological society engineering group working party report. *Q. J. Eng. Geol. Hydrogeol.* **1990**, *23*, 4–101. [CrossRef]
43. Ding, L.; Zhang, J.; Zhou, C.; Han, S.; Du, Q. Particle breakage investigation of construction waste recycled aggregates in subgrade application scenario. *Powder Technol.* **2022**, *404*, 117448. [CrossRef]
44. Xiao, Y.; Kong, K.; Aminu, U.; Li, Z.; Li, Q.; Zhu, H.; Cai, D. Characterizing and Predicting the Resilient Modulus of Recycled Aggregates from Building Demolition Waste with Breakage-Induced Gradation Variation. *Materials* **2022**, *15*, 2670. [CrossRef]
45. Pierozan, R.C.; Araujo, G.L.S.; Palmeira, E.M.; Romanel, C. Influence of variables related to soil weathering on the geomechanical performance of tropical soils. *J. Rock Mech. Geotech. Eng.* 2023; 15, *in press*.
46. *ASTM D5550-06*; Standard Test Method for Specific Gravity of Soil Solids by Gas Pycnometer. The American Society for Testing and Materials: West Conshohocken, PA, USA, 2015; pp. 1–5. [CrossRef]
47. *ASTM C136/C136M-14*; Standard Test Method for Sieve Analysis of Fine and Coarse Aggregates. The American Society for Testing and Materials: West Conshohocken, PA, USA, 2020; pp. 1–5. [CrossRef]
48. *ASTM D7928-21e1*; Standard Practice for Particle-Size Distribution (Gradation) of Fine-Grained Soils Using the Sedimentation (Hydrometer) Analysis. The American Society for Testing and Materials: West Conshohocken, PA, USA, 2021; pp. 1–27. [CrossRef]
49. *ASTM D4221-18*; Standard Test Method for Dispersive Characteristics of Clay Soil by Double Hydrometer. The American Society for Testing and Materials: West Conshohocken, PA, USA, 2018; pp. 1–5. [CrossRef]
50. *ASTM D4253-16e1*; Standard Test Methods for Maximum Index Density and Unit Weight of Soils Using a Vibratory Table. The American Society for Testing and Materials: West Conshohocken, PA, USA, 2019; pp. 1–14. [CrossRef]
51. *ASTM D4254-16*; Standard Test Methods for Minimum Index Density and Unit Weight of Soils and Calculation of Relative Density. The American Society for Testing and Materials: West Conshohocken, PA, USA, 2016; pp. 1–9. [CrossRef]
52. *ASTM D698-12*; Standard Practice for Laboratory Compaction Characteristics of Soil Using Standard Effort (12,400 ft-lbf/ft^3 (600 kN-m/m^3)). The American Society for Testing and Materials: West Conshohocken, PA, USA, 2021; pp. 1–13. [CrossRef]
53. *ASTM D4318-17e1*; Standard Test Methods for Liquid Limit, Plastic Limit, and Plasticity Index of Soils. The American Society for Testing and Materials: West Conshohocken, PA, USA, 2018; pp. 1–20. [CrossRef]
54. *ASTM C535-16*; Standard Test Method for Resistance to Degradation of Large-Size Coarse Aggregate by Abrasion and Impact in the Los Angeles Machine. The American Society for Testing and Materials: West Conshohocken, PA, USA, 2016; pp. 1–3. [CrossRef]
55. *ASTM D2487-17*; Standard Practice for Classification of Soils for Engineering Purposes (Unified Soil Classification System). The American Society for Testing and Materials: West Conshohocken, PA, USA, 2020; pp. 1–10. [CrossRef]

56. *ASTM D3080/D3080M-11*; Standard test method for direct shear test of soils under consolidated drained conditions. The American Society for Testing and Materials: West Conshohocken, PA, USA, 2011; pp. 1–9. [CrossRef]
57. Lo Presti, D.C.F.; Pedroni, S.; Crippa, V. Maximum dry density of cohesionless soils by pluviation and by ASTM D4253-83: A comparative study. *Geotech. Test J.* **1992**, *15*, 180–189. [CrossRef]
58. Schlosser, F.; Bastick, M. Reinforced earth. In *Foundation Engineering Handbook*, 1st ed.; Fang, H.Y., Ed.; Springer: New York, NY, USA, 1991; pp. 778–795. [CrossRef]
59. Georgiou, I.; Loli, M.; Kourkoulis, R.; Gazetas, G. Pullout of steel grids in dense sand: Experiments and design insights. *J. Geotech. Geoenviron.* **2020**, *146*, 1–19. [CrossRef]
60. Kido, R.; Kimura, M. Investigation of soil deformation characteristics during pullout of a ribbed reinforcement using X-ray micro CT. *Soils Found.* **2021**, *61*, 642–657. [CrossRef]
61. Kumar, V.K.; Ilamparuthi, K. Performance of anchor in sand with different forms of geosynthetic reinforcement. *Geosynth. Int.* **2020**, *27*, 503–522. [CrossRef]
62. AASHTO. *LRFD Bridge Design Specifications*, 9th ed.; American Association of State Highway and Transportation Officials: Washington, DC, USA, 2020; pp. 1–1912.
63. Lawson, W.D.; Jayawickrama, P.W.; Wood, T.A.; Surles, J.G. Pullout Resistance Factors for Inextensible Mechanically Stabilized Earth Reinforcements in Sandy Backfill. *Transp. Res. Rec.* **2013**, *2363*, 21–29. [CrossRef]
64. Huang, B.; Bathurst, R.J.; Allen, T.M. LRFD Calibration for Steel Strip Reinforced Soil Walls. *J. Geotech. Geoenviron.* **2012**, *138*, 922–933. [CrossRef]
65. Jayawickrama, P.W.; Lawson, W.D.; Wood, T.A.; Surles, J.G. Pullout Resistance Factors for Steel MSE Reinforcements Embedded in Gravelly Backfill. *J. Geotech. Geoenviron.* **2015**, *141*, 04014090. [CrossRef]